Promoting Methanol Synthesis and Inhibiting CO_2 Methanation with Bimetallic In-Ru Catalysts

Feiyang Geng, [a] *Xun Zhan,* [b] *and Jason C. Hicks* [a]*

[a] Department of Chemical and Biomolecular Engineering, University of Notre Dame, Notre Dame, Indiana 46556, United States

[b] Bloomington Electron Microscopy Center, Indiana University, Bloomington, Indiana 47405, United States

ABSTRACT

In this work, we investigated the promotional effects of In on Ru for the synthesis of methanol via CO_2 hydrogenation in the liquid phase. Incorporation of In to Ru results in a methanol selectivity of ~85% at 240 °C and 3.4 MPa (CO_2/H_2=1/3). After incorporation of either promoter, no methane was observed under the conditions studied (200-240 °C). The combination of In and Ru modulates Ru sites geometrically and electronically. X-ray diffraction and x-ray photoelectron spectroscopy provided evidence of the structural evolution from mixed metal oxides to alloy and intermetallic phases and charge transfer from In to Ru, respectively. Additionally, in-situ diffuse reflectance infrared Fourier transform spectroscopy studies using probe molecules (CO_2+H_2, CO, formic acid, methanol), as well as CO-temperature programmed reaction and H_2-D_2 exchange experiments, were conducted to provide insight to the promotional effect of In. With the incorporation of In, surface formate and methoxy species were stabilized to promote the formation of methanol. Methanation, which is a dominant pathway on monometallic Ru, was inhibited with promoter addition.

Key Words: Bimetallic, Promoters, Indium, Ruthenium, Methanol, CO_2 hydrogenation.

INTRODUCTION

The efficient conversion of carbon dioxide (CO_2) with renewable hydrogen has the potential to recycle CO_2 as a versatile C1 building block for the synthesis of a valuable suite of products, while potentially lowering the greenhouse gas concentration in the atmosphere.[1-5] The conversion of CO_2 to methane (CH_4) has a low Gibbs free energy below 500 ºC and is the most thermodynamically favored product from CO_2 hydrogenation when comparing CH_4, carbon monoxide (CO), and CH_3OH.[6] Of these three products, CH_3OH is a more valuable platform chemical and can also serve as a hydrogen storage medium.[7] Commercial CH_3OH synthesis catalysts typically require a high H_2/CO_2 ratio (H_2:CO_2≥3) and high pressure (> 10 MPa) to improve the methanol selectivity, which increases processing costs.[8, 9] Therefore, the identification of new catalyst compositions that avoid methane formation while maximizing CH_3OH yields during CO_2 hydrogenation with lower H_2/CO_2 ratio remains a significant challenge.

Ruthenium (Ru) nanoparticle and/or nanocluster catalysts have been extensively studied as highly active catalysts for CO_2 methanation.[1, 10, 11] Ru catalysts have CH_4 selectivity of nearly 100% at full conversion with a methanation onset temperature as low as 60 ºC.[8, 12] At higher temperatures (~450 ºC), 99% CH_4 selectivity has also been reported on Ru-based catalysts.[13] Efforts to modulate the selectivity of Ru catalysts for methanol synthesis have been made through the development of soluble, molecular catalysts.[14] However, soluble catalysts often suffer from limited thermal stability and difficulty when separating from the product to reuse/recycle.[15, 16] Alternatively, Ru performance can be modulated through the addition of promoters through electronic and geometric effects. Such approaches have been successful with In-Pd and In-Rh alloys, where In was predicted to prohibit the CO methanation pathway.[9, 17, 18] However, the methanol selectivity for reduced In-Pd alloys was 13%, due to the significant contribution from the reverse water gas shift reaction.[18] It was suggested that the interface between the indium oxide and alloy plays a key role in increasing the methanol selectivity.[7] Li et al. recently reported the promotional effects of supporting Ru on indium oxide to increase the methanol selectivity compared to Ru/Al_2O_3.[9] However, methanation was observed with a CH_4 selectivity of < 20%. The intermetallic phases of In_xRu_y (In_3Ru_1 and In_1Ru_3) were discovered in 1964, and additional studies on the thermoelectric properties and theoretical electronic structure have been reported.[19-21] The In_3Ru_1 phase, in particular, contains Ru sites isolated by 8 In atoms with shorter In-Ru distance than Ru-Ru, [21, 22] and its band structure is modified with the incorporation of In. Performance of these intermetallic materials and the alloy form of In-Ru is largely unknown, and the unique geometric and electronic structures might open up new opportunities for the selective of methanol.

In this paper, we focus on the evaluation of Ru promoter (In)for the synthesis of methanol from H_2/CO_2. We prepared silica (SiO_2)-supported In-Ru bimetallic catalysts with various ratios and different reduction temperatures to compare the catalytic performance. Our work highlights the incorporation of In prevents methanation between 200-240 ºC and 3.4 MPa, while the methanol selectivity remains high (75-85% at 240 ºC). In order to understand the synergistic effects of In incorporation, chemisorption probe molecules (e.g., CO, methanol, formic acid) were utilized to understand the interaction between surface Ru sites and adsorbates before and after the incorporation of In. H_2 activation and CO hydrogenation, which serve as critical steps for methanation, were also investigated. These results provide further insight into how the bimetallic composition influences the stability of potential surface intermediates and inform the proposed reaction pathways towards methanol synthesis.

EXPERIMENTAL DETAILS

Materials

Fumed SiO_2 (Aerosil(R) 200, SiO_2 >99 %, surface area 175 - 225 m^2/g), Silica gel (Sigma-Aldrich, Davisil Grade 635), $RuCl_3 \cdot xH_2O$ (Oakwood Chemicals, 99%), $Ni(NO_3)_3 \cdot 6H_2O$ (Alfa Aesar, 98%), $In(NO_3)_3 \cdot xH_2O$ (Alfa Aesar, 99.999%), commercial $Cu/Zn/Al_2O_3/MgO$ (Alfa Aesar, 63.5 wt% CuO, 20 wt% ZnO, 10 wt% Al_2O_3 and 1.5 wt% MgO), 1,4-dioxane (ACROS Organics, 99 %, water 50 ppm max), formic acid (Alfa Aesar, 97 %), CO_2 (Airgas, 99.99 %) H_2 (Airgas, 99.999 %), D_2 (Airgas, 99.999 %), N_2 (Airgas, 99.998 %), 30% CO in He (Airgas, 99.99 %), 1%O_2 in He (Airgas, 99.99 %). All chemicals were used without further purification.

Catalyst synthesis

The SiO_2 supported Ru and In-Ru bimetallic catalysts were synthesized through incipient wetness impregnation. Specially, 2.03 g of fumed SiO_2 were calcined at 200 ºC for 5 h and cooled overnight before use. For the $In_{0.85}Ru_1$ sample, the precursor solution was made by dissolving

0.2444 g of $RuCl_3 \cdot xH_2O$ and 0.3082 g of $In(NO_3)_3 \cdot xH_2O$ in 4.7 g DI water. The solution was added dropwise onto the fumed SiO_2 and well-mixed. Then, the wet sample was sonicated for 15 min and placed in air at room temperature for 24 h. The dried sample was ground and subsequently calcined at 400 °C for 1 h to remove residual chlorine. This precursor was transferred to the tube furnace for reduction in pure H_2 (160 ml/min H_2) with a ramp rate of 5°C/min. The precursor was heated to 100 °C first and held for 1h. The temperature was subsequently increased to and held at the final temperature for 2 h (only 1h for $In_{0.85}Ru_1$-300/450). Materials with a final reduction temperature of 800 °C were denoted $In_{0.85}Ru_1$-800. The $In_1Ni_{0.9}$ sample was synthesized in the same way as previously reported,[7] and it was reduced at 300 °C for 1 h (named as $In_1Ni_{0.9}$-300). The commercial $Cu/Zn/Al_2O_3/MgO$ catalyst was reduced at 290 °C for 2 h before use. After the reduction, all the catalysts were cooled to room temperature, passivated with a flowing stream of 1 % O_2/He for 1h, and then transferred to the N_2 drybox for storage.

Material Characterization

The structure of the as-synthesized catalysts was determined by powder X-ray diffraction (XRD) with a Bruker D8 Advance Davinci instrument (Cu Kα X-ray source). Samples were pressed into the sample holder and rotated at a speed of 15 °/min with an increment size for each measurement of 0.02 °/step.

HRTEM (high-resolution TEM) and STEM-HAADF (high-angle annular dark-field) were utilized to provide information about particle size distribution and crystal structure. The samples were prepared by drop casting onto carbon-coated copper grids. Images were collected with JEOL 3200FS, operating at 300 kV. The JEOL 3200FS was equipped with an Oxford XEDS (X-ray energy dispersive spectroscopy) detector for elemental concentration measurements and mapping.

Inductively coupled plasma – optical emission spectroscopy (ICP-OES; PerkinElmer Optima 8000) with using external calibration curves for each element of interest was utilized to determine the composition of the as-synthesized bimetallic and monometallic catalysts. All bimetallic samples can be easily dissolved in aqua regia after heating at 200 ^{o}C for 3 h while supported Ru can be hardly digested until temperature reaches 220 ^{o}C and holds for 24 h. The metal ratios and loadings are listed in Table S1. In-Ru bimetallic catalysts show a slight In deficiency compared to the nominal ratio. For simplicity, the catalysts are named based on their nominal ratios, and the mass normalized reaction rates are calculated based on measured metal loading.

X-Ray Photoelectron Spectroscopy (XPS) was performed on both Ru and bimetallic catalysts that were reduced at 800 ^{o}C. Prior to measurement, the samples were pressed to form a thin wafer. Powdered Si(111) was added as reference material, and the Si $2p_{3/2}$ peak was shifted to 99.3 eV. The Si $2p_{3/2}$ peak was used instead of C1s peak because the binding energy of C1s peak (from the carbon tape) at 284.8 eV overlapped with Ru 3d features. As is shown in Fig. S3, the peaks in Ru 3d region (280~288 eV) was deconvoluted to Ru $3d_{3/2}$ (blue) at around 280 eV together with Ru $3d_{5/2}$ (purple) and C1s features from carbon tap (pink and green). Meanwhile, the In 3d region (441~456 eV) was deconvoluted to In $3d_{5/2}$ at around 444 eV and In$3d_{3/2}$ at 451 eV.

H_2-O_2 titration was performed with a Quantachrome Autosorb IQ-C-XR Gas Sorption Analyzer. In a typical process, 150 mg sample was loaded in a U shape sample tube and reduced identically to the catalyst synthesis procedure. After reduction, the sample was cooled to 25 ^{o}C and a flow of 1 % O_2/He was used to oxidize surface Ru site for 1 h. Then, He was used to purge the system for 1h, and the sample was subsequently heated to 300 ^{o}C and evacuated for 24h. After evacuation, the sample was cooled to 100 ^{o}C to perform the H_2 titration experiment to minimize physiosorbed H_2 and also facilitate the reduction of RuO_2.[23] The resulting isotherm curve was summarized in Fig.

S1. After the titration, the total amount of adsorbed H_2 was determined by extrapolation of isotherm curve to zero pressure and number of Ru sites was calculated based on Kubicka's work that 2.5 H_2 molecules titrated 1 oxidized Ru site.[23] It is worth mentioning that the total amount of H_2 may contain reversible adsorbed H_2 which might overestimate the Ru site density. CO titrations were also performed on the reduced In-Ru samples. However, no detectable CO uptake was observed due to the low Ru site density and weak CO adsorption on In-enriched surfaces.[18]

The site density for $Cu/ZnO/Al_2O_3/MgO$ was determined through a H_2 TPD experiment as reported in literature.[24] The amount of H_2 was quantified via mass spectrometry through an external calibration curve on m/z=2. In a typical experiment, 150 mg of a 290 °C pre-reduced sample was loaded in the U shape sample tube and reactivated in 30 ml/min H_2 flow at 220 °C for 2 h. After H_2 reduction, the sample was cooled in a -40 °C bath (75% isopropanol + 25% water + dry ice) for 1 h to adsorb H_2. A liquid nitrogen bath was then used, and the sample was quickly cooled to 77 K and held for 1h. The gas was switched to He and purged for 1 h. The cooling bath was then removed to allow the temperature to rise spontaneously. Once the temperature rose to room temperature, a heating mantle was applied and ramped to 100 °C to facilitate H_2 desorption. The total H_2 was determined to be 55 umol/g, which is close to the literature value for $Cu/ZnO/Al_2O_3$.[24] Assuming H/Cu ratio is 0.4,[24] the total Cu site density was measured as 285 μmol/g.

H_2-D_2 exchange experiments were conducted to investigate the activation of H_2 on Ru-800 and In_3Ru_1-800 using mass spectrometry to determine the concentration change of HD (m/z=3), H_2 (m/z=2) and D_2 (m/z=4). Approximately 100mg of pre-reduced sample was loaded in a U-shape sample tube and purged with 30 ml/min H_2 flow for 1 h to remove air. Then 30 ml/min H_2 + 30 ml/min D_2 was fed together into the sample while a liquid nitrogen bath was used to cool the sample to 77 K.

In-situ diffuse reflectance infrared Fourier transform spectroscopy (DRIFTS) investigations were performed using a Bruker Vertex 70 spectrometer equipped with a mercury cadmium telluride detector. Before CO adsorption, materials were treated with He at 300°C for 1 h and then cooled to room temperature. Ru-800 was reduced in H_2 at 300 °C for 1 h and subsequently purged with He at the same temperature for 1 h. After cooling the sample to 25 °C, 30 ml/min 30 % CO/He was introduced into the sample cell for 30 min and then purged with He to remove the residual CO. Measurements were taken every 3 min with resolution of 4 cm^{-1}. Formic acid and methanol vapor adsorption experiments were also performed. For these experiments, 30 ml/min He was used to carry formic acid or methanol vapor from a glass bubbler to the sample cell at room temperature. After saturation for 30 min, the sample was purged with He for 30 min and then switched to H_2 while heating to the target temperature.

Temperature programmed reduction (TPR) experiments were conducted on a Micromeritics Chemisorb 2750 equipped with mass spectrometry analysis capabilities. Approximately 150 mg of sample was loaded in a U shape tube and placed in 40 ml/min 5% H_2/Ar for at least 1 h prior to the test. During TPR, the sample was ramped to 800 °C with a heating rate of 5 K/min. CO temperature programmed reaction (TPRx) was performed on the same instrument. Approximately 100 mg of sample was reduced at 800 °C for 2 h and then purged with He for 0.5 h at the same temperature. The sample was then cooled to 30 °C for CO adsorption. A total of 1.59 ml of 30 % CO was injected into the sample to reach saturation. Then, the gas stream was switched to H_2 and ramped to 700 °C at a rate of 20 °C/min. The m/z=15 and 16 ion currents were utilized to monitor methane formation.

Catalysis Activity Measurement

All reactions were conducted in a 50 mL Parr batch reactor equipped with a programmable temperature controller and pressure indicator. We evaluated the catalysts in 1,4-dioxane due to its higher CO2 solubility than hydrogen solubility.[25, 26] It is also worth noting that the solvent may also assist in hydride transfer [27, 28] and formation of carbonate [29, 30] which can alter the catalytic performance. We also tested isopropanol as an alternative solvent, which resulted in a similar CH_3OH selectivity (98% CH_3OH, 2% CO) as 1,4-dioxane (95% CH_3OH, 5% CO and trace amount of methyl formate) after 13h reaction at 200 °C with 100 mg In_3Ru_1-800, 15 ml solvent and 6.7 MPa reactant ($N_2/CO_2/H_2$ = 1/10/30). For each experiment, 20 ml of anhydrous 1,4-dioxane was used as the solvent with 100 mg of the catalyst. The reactor was purged with N_2 three times, purged with H_2 once, and purged with CO_2 three times before charging the reactants. Approximately 0.48 MPa of CO_2 was initially charged in the reactor, followed by 0.34 MPa of N_2 and 1.44 MPa of H_2 at room temperature. The reactor was heated to 240 °C within 20 min and stirred at 690 rpm. The total pressure at 240°C was ~5.2 MPa with 1.8 MPa 1,4-dioxane vapor + N_2 based on GC analysis. For the commercial $Cu/ZnO/Al_2O_3/MgO$ catalyst, the formation of products were observed during the heating process. Therefore, only CO_2 and N_2 were charged into the reactor at room temperature. Afterwards, H_2 was added at 240 °C to initiate the reaction. After the experiments, the reactor was cooled in an ice bath for 30 min. The gas was expanded slowly into a 500 ml empty cylinder so that the majority of CO_2 present in the liquid phase was extracted to the gas phase. The collected gas was sent to a GC TCD/FID for quantification of N_2, CH_4, CO and CO_2. The liquid phase was recovered at the bottom of the reactor, and the CH_3OH concentration was quantified using an Agilent 7890b GCMS using an external calibration curve. The CH_3OH formation rate was calculated by the total moles of CH_3OH produced per gram of catalyst and reaction time at 240 °C.

The CO_2 conversion was calculated by the total amount of products (CH_3OH, CO, CH_4) divided by the total amount of CO_2. The carbon balance was also calculated and summarized in Table S2.

RESULTS

Structural Characterization and Reducibility of Catalysts

XRD was used to understand the crystal structure of the 800 °C reduced bimetallic and monometallic catalysts. **Figure 1** (a) shows an In_3Ru_1 intermetallic phase (PDF card 04-007-4636) was formed on all In-Ru bimetallic samples, including $In_{0.85}Ru_1$-800 (In:Ru = 0.85:1), In_2Ru_1-800 (In:Ru = 2:1) and In_3Ru_1-800 (In:Ru = 3:1). No In_2O_3 was observed from XRD on these samples. Residual Ru phase was detected (44 °) and decreased relative to the In_3Ru_1 phase as the In/Ru ratio increased, which showed In addition promoted the conversion of Ru into the In_3Ru_1 intermetallic phase.

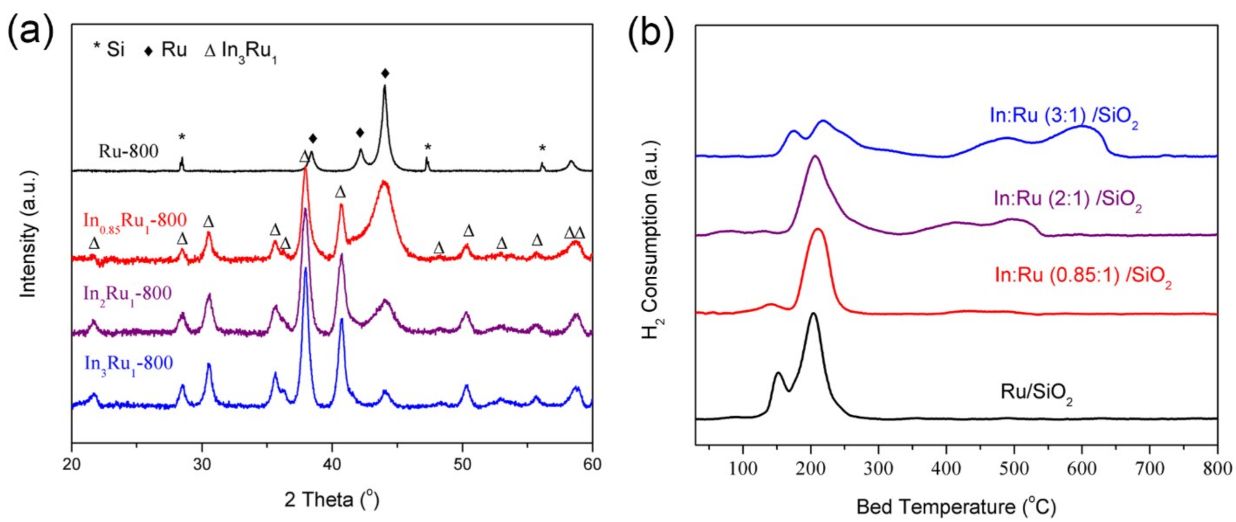

Figure 1. (a) XRD pattern of 800 °C reduced Ru and In-Ru bimetallic catalysts. (b) TPR profile of bimetallic and monometallic catalysts

To determine the reducibility of bimetallic samples, temperature programmed reduction (TPR) was performed on Ru/SiO_2 and In-Ru bimetallic catalysts. Figure 1 (b) shows the reduction of Ru occurred between 100 and 300 °C, evidenced by two hydrogen consumption peaks centered around 150 °C and 200 °C consistent with literature results [9, 10]. With a catalyst composition having a nominal In/Ru ratio less than 1, similar peaks are observed between 100 and 300 °C, suggesting $In_{0.85}Ru_1$ is reduced below 300 °C. XRD analysis was performed on pre-reduced $In_{0.85}Ru_1$ as well as $In_{0.85}Ru_1$ reduced at 300 °C, 450 °C and 800 °C to provide additional evidence. Prior to reduction, $In_{0.85}Ru_1$ is clearly a mixture of In_2O_3 and RuO_2 phase. After reduction at 300 °C, only one broad diffraction peak at 42.5 ° can be observed which is close to the (101) facet of pure Ru at 44 °(Figure S3). No In_2O_3 phase was observed and is consistent with the TPR result. As the reduction temperature is increased to 450 °C, the In_3Ru_1 intermetallic phase appears as well as the residual alloy phase at 43.74 °. After reduction at 800 °C for 2h, $In_{0.85}Ru_1$-800 shows the same In_3Ru_1 phase as $In_{0.85}Ru_1$-450 while its crystallite size increases from 11 nm to 15 nm. Additionally, the alloy peak shifts to 44.04 ° (800 °C) which is in the same position as pure Ru.

As In becomes more enriched than Ru (In/Ru=2 and 3), TPR shows low temperature peaks (<300 °C) shift to higher temperature than $In_{0.85}Ru_1$, and two reduction peaks between 400-700 °C becomes significant which indicates the excess of bulk In_2O_3 is not fully reduced until T=~700 °C. Clearly, addition of Ru improves the reducibility of catalyst, consistent to the TPR results of In-Pd bimetallic catalysts.[7]

Thus, the TPR experiments coupled with XRD analysis show that reduction at 800 °C is capable of fully reducing In enriched samples while 300 °C is high enough to reduce the pure Ru and In deficient samples.

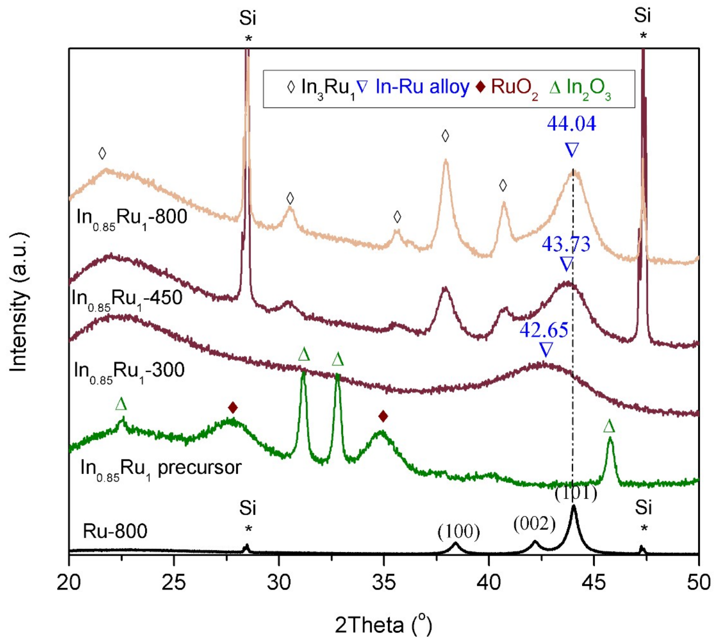

Figure 2. XRD pattern of pre-reduced $In_{0.85}Ru_1$ (so called "$In_{0.85}Ru_1$ precursor"), $In_{0.85}Ru_1$ sample reduced at various temperatures ($In_{0.85}Ru_1$-300/450/800) and Ru-800. Pure silicon was used as a reference.

Effect of In Promoter on the Catalytic Performance of Ru

We begin by providing catalytic results from synthesized bimetallic catalyst, In_3Ru_1. The In_3Ru_1 phase is commonly reported as a stable In-Ru intermetallic phase with a tetragonal structure.[22] Thus, we synthesized the catalyst with a nominal In/Ru ratio of 3, and XRD was used to confirm the formation of this intermetallic phase after reduction at 800 °C (Figure 1(b)). Catalyst evaluation was carried out at 240 °C and 3.4 MPa with 100 mg of bimetallic catalyst or 5 mg monometallic catalyst (metal loadings on SiO_2: In_3Ru_1: 8.5 wt %, Ru: 11.1 wt %) so that the temperature was within the range of the commercial process (200-300 °C) and the pressure was at the low limit of commercial condition (3.5-10 MPa). Table 1 summarizes the performance of the catalysts after a 3.5 h reaction. Interestingly, In incorporated catalysts show no methane production. Further, In_3Ru_1-800 has a significantly higher methanol selectivity of 86% compared to Ga_3Ru_1-800, which formed no methanol. To make a similar comparison to the In_3Ru_1-800 catalyst, 4.5% In_2O_3/SiO_2 was reduced at 800 ºC, and the resulting In catalyst showed no activity. As a control experiment, a blank reaction with the catalysts in the 1,4-dioxane solvent was also conducted to determine if any solvent degradation occurred simultaneously under the same pressure of H_2. After 3.5 hours of reaction time, In-Ru catalysts do not produce CH_3OH, and only trace amounts of CO and CO_2 were observed. Comparably, Ru-800 displayed significant 1,4-dioxane degradation, forming >99% CH_4 (1.4 mmol) and a trace amount of CO, which is consistent with the work by T Hara et al.[31] Further, the addition of CO_2 enhanced the production of CH_4 by 27% with Ru-800, demonstrating that CO_2 hydrogenation to CH_4 remains the dominant reaction pathway over the Ru-800 catalyst. More importantly, it shows that (1) addition of In significantly modifies the catalytic behavior such that severe solvent decomposition is prevented and (2) since solvent decomposition to CH_4 is not observed with the bimetallic compositions, any residual Ru from incomplete In-Ru bimetallic compound formation is unlikely to be the dominant active site, as seen with In-Pd alloys.[13]

Table 1. Catalytic performance of bimetallic and monometallic catalysts at 240 ºC, 3.4 MPa (3/1 H_2/CO_2).

Catalyst	CH_3OH selectivity (%)	CO selectivity (%)	CH_4 selectivity (%)	Mass normalized activity (mmol/g_{metal}/h)[a]
In_3Ru_1-800	86	14	0	278

Ru-800	2	<0.1	98	22200
In_2O_3/SiO_2 reduced at 800 ºC	-	-	-	0

a Reaction time of 3.5 hours after removing the solvent degradation products from background reactions.

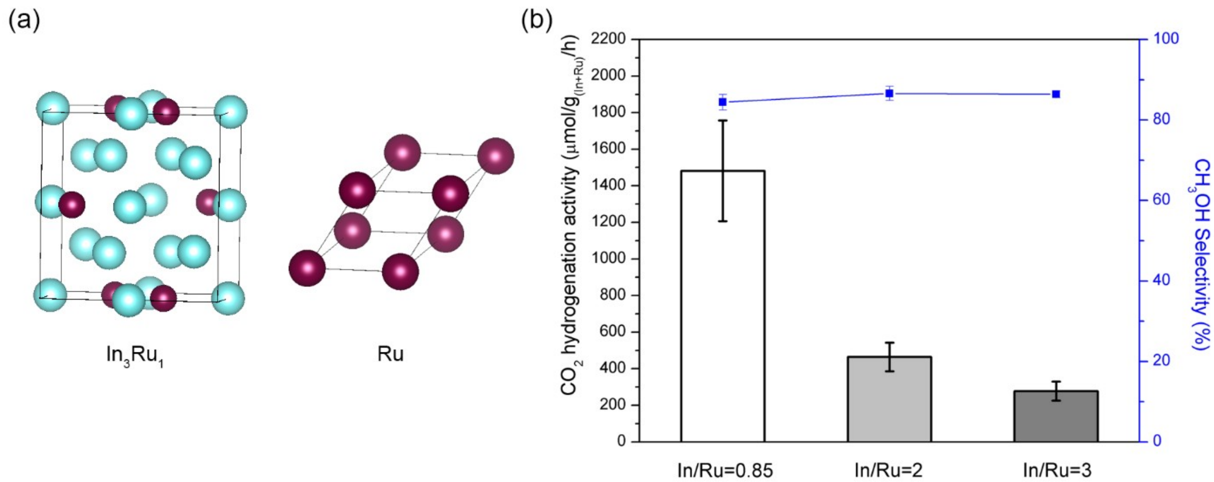

Figure 3. (a) crystal structure of In_3Ru_1 and Ru phase[32] (magenta is Ru and blue is In) (b) Influence of In/Ru ratio on catalytic activity at 3.5h, 240 ºC and 3.4 MPa (3/1 H_2/CO_2).

With the remarkable selectivity of the In promoted catalyst, we varied the In/Ru ratio to investigate the effect of composition on the catalytic performance. Figure 3 shows the bimetallic structures (Figure 3a) and the mass normalized CO_2 consumption rates and CH_3OH selectivity of In-Ru catalysts after a 3.5 h reaction (Figure 1b). Similar to the results with In_3Ru_1-800, only CO was observed in the gas phase for the higher Ru compositions. All three In_xRu_1-800 samples also exhibited similar CH_3OH selectivity (84-86%). However, the mass normalized CO_2 consumption rate increases substantially as the In/Ru ratio decreases, which indicates the In content suppresses the catalyst activity.

Effect of Reduction Temperature on the Performance of $In_{0.85}Ru_1$ Catalysts

The CH_3OH selectivity was nearly invariant with the different In/Ru ratios, but the CO_2 consumption rate was highest with the $In_{0.85}Ru_1$-800 catalyst. We subsequently examined structure-performance relationships by varying the reduction temperature of the $In_{0.85}Ru_1$ catalyst (In loading 4.2%). $In_{0.85}Ru_1$ samples were synthesized at different temperatures (300 °C, 450 °C, 800 °C) to yield three catalysts for comparison: (1) $In_{0.85}Ru_1$-300, (2) $In_{0.85}Ru_1$-450, and (3) $In_{0.85}Ru_1$-800. The catalytic results at 240 °C and 3.4 MPa ($3H_2/1CO_2$) are presented in Figure 4. Significant changes can be observed on the mass normalized CH_3OH production rates (Figure 4a). The $In_{0.85}Ru_1$-300 showed the lowest CH_3OH productivity among the three samples, with $In_{0.85}Ru_1$-450 at the highest CH_3OH productivity. Although the CH_3OH productivity for $In_{0.85}Ru_1$-800 was less than that of $In_{0.85}Ru_1$-450, it was 2x more active than $In_{0.85}Ru_1$-300. Ru site-normalized CH_3OH production rates were calculated by using H_2-O_2 titration experiments. We observe the same trend as the mass normalized rates (Figure 4 (a and b)), which implies the reduction condition strongly influences the intrinsic activity of Ru. In terms of their product selectivity after 3.5 h of reaction time, the CH_3OH selectivity varies between 81 to 85% with CO as a minor product, which is much less than the variation in CH_3OH production rates. For each catalyst, no methane was observed in the product stream regardless of the reduction temperature and resulting crystal structure. In order to evaluate the influence of residual In_2O_3 to the total activity of the catalyst, In_2O_3 was supported on fumed SiO_2 with the same In loading (4.5%), calcined at 400 °C, and evaluated at the same condition. The CH_3OH productivity was 10.9 μmol/g_{cat}/h for In_2O_3/SiO_2, which is significantly lower than all of the $In_{0.85}Ru_1$ catalysts; however, the CH_3OH selectivity was 85%, which is similar to other reports.[33, 34] Therefore, the contribution of residual In_2O_3 to the total activity of the catalyst is insignificant.

Benchmarking In-Ru catalysts

The CO_2 conversion profiles as a function of reaction time and CH_3OH selectivity at various CO_2 conversions at 240 ºC are provided in Figure 4 (c) and (d), respectively. To benchmark the catalysts, two of the most active In-Ru catalysts ($In_{0.85}Ru_1$-800 and $In_{0.85}Ru_1$-450) were benchmarked with two highly active catalysts: 1) $Cu/ZnO/Al_2O_3/MgO$[35] and 2) $In_1Ni_{0.9}$-300.[18] $In_1Ni_{0.9}$ formed predominantly CO as the product with less than 30% CH_3OH at 240 ºC, which is qualitatively consistent with previous studies.[18] The $Cu/ZnO/Al_2O_3/MgO$ catalyst showed 54% CH_3OH selectivity at ~1% conversion, which decreased to ~35% CH_3OH selectivity at ~6% conversion with CO as the only byproduct. A similar trend was observed by Chang et al. on Cu/CeTiO, where the CH_3OH selectivity decreased nonlinearly as the CO_2 conversion increased (235ºC and 3MPa).[36]

The selectivity to CH_3OH with $In_{0.85}Ru_1$-800 at conversions below 5% is also shown in Figure 4 (d). The CH_3OH selectivity at low conversion (<1%) is nearly 85% with only CO as a minor product. At 3% conversion, the CH_3OH selectivity decreased to 75%. Figure 4 (d) also shows the CH_3OH selectivity as a function of CO_2 conversion for $In_{0.85}Ru_1$-450, which follows the same trajectory as $In_{0.85}Ru_1$-800. Comparably, the commercial catalyst and $In_1Ni_{0.9}$ catalyst have much lower CH_3OH selectivity in the same range of CO_2 conversion. Therefore $In_{0.85}Ru_1$ shows an advantage over both materials.

In terms of the catalytic activity, $Cu/ZnO/Al_2O_3/MgO$ has the highest mass normalized CH_3OH production rate (11.2 mmol/g_{cat}/h). Comparably, the rate for $In_{0.85}Ru_1$-450 and $In_1Ni_{0.9}$-300 catalysts are 0.49 and 0.24 mmol/g_{cat}/h, respectively. After normalizing the catalytic activity at 3.5 h by the number of titrated sites from H_2-O_2 experiments (6 umol Ru site/g for $In_{0.85}Ru_1$-450 and 285 umol Cu site/g for Cu/ZnO/Al_2O_3/MgO), the site-time yield (STY) of CH_3OH for $In_{0.85}Ru_1$-450 is 81.9 mmol CH_3OH/mmol site/h, which is much higher than the STY of the commercial catalyst (39.6 mmol CH_3OH/mmol site/h), as shown in Table 2.

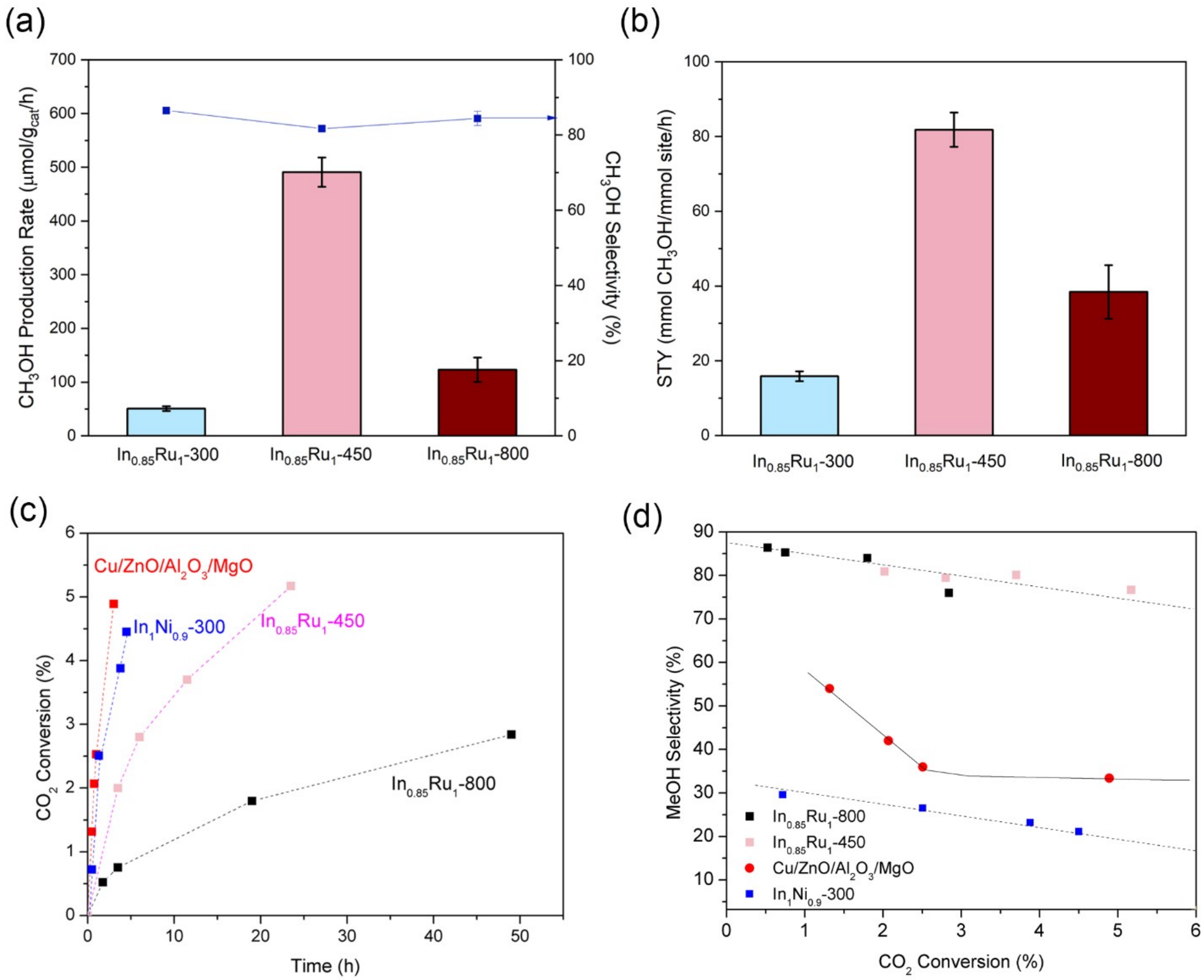

Figure 4. (a) Effect of reduction temperature on the mass normalized CH_3OH production rate of $In_{0.85}Ru_1$ at 3.5 h, (b) effect of reduction temperature on the Ru site normalized activity of $In_{0.85}Ru_1$,

(c) CO_2 conversion vs. time for various catalysts, and (d) CH_3OH selectivity vs. CO_2 conversion for various catalysts.

Table 2. Methanol selectivity and catalyst activity comparisons at 240 °C

Catalyst	CH_3OH selectivity[a] (%)	Site density (μmol/g)	Mass normalized CH_3OH production rate[b] (mmol/g_{cat}/h)	STY of CH_3OH[b] (mmol CH_3OH/mmol site/h)	Site normalized CO_2 hydrogenation activity[b] (mmol CO_2/mmol site/h)
$Cu/ZnO/Al_2O_3/MgO$	42	285	11.3	39.6	118
$In_{0.85}Ru_1$-450	82	6	0.49	81.9	100
$In_1Ni_{0.9}$-300	27	N/A[c]	0.24	N/A[c]	N/A[c]

[a] Evaluated at 2-2.5% conversion

[b] Evaluated at 3.5 hours.

[c] For $In_1Ni_{0.9}$-300, the synergy between In-Ni intermetallic phase and In_2O_3 was claimed to be the key to the catalytic activity.[18] Therefore, Ni sites titrated by H_2 do not represent the true active site of the catalyst and here STY for $In_1Ni_{0.9}$-300 is not listed.

Surface Analysis of the Supported Catalysts

To probe the effect of promoter addition on the electronic properties of the catalysts, XPS was performed on Ru-800, In-800 andIn_xRu_1-800samples. Figures 5 (a) and (b) show the $In3d_{5/2}$ of $In_{0.85}Ru_1$ is 1 eV higher than metallic In, while the $Ru3d_{5/2}$ of $In_{0.85}Ru_1$ is at similar binding energy as monometallic Ru. As the In/Ru ratio was increased to 3, the $In3d_{5/2}$ was 0.3 eV higher than metallic In and 0.3 eV lower than In_2O_3, and $Ru3d_{5/2}$ was ~0.2 eV lower than metallic Ru. The charge transfer from In to Ru therefore resulted in partial oxidation of In and partial reduction of Ru for the In-Ru bimetallic catalysts. At 800 °C, it has been reported that In_2O_3 can be reduced and reduction temperature of In can decrease due to addition of noble metal.[18, 37] This was confirmed by analyzing the $In3d_{5/2}$ region of In_2O_3/SiO_2 reduced at 800 °C, which was centered at 444.2 eV (In(0) is reported at ~444 eV and In_2O_3 is reported at ~445 eV[38, 39]) Similar to In, recent work by H. Hosono et al. with the YRu_2 intermetallic phase showed similar charge transfer from Y to Ru, which is consistent with our observations.[40]

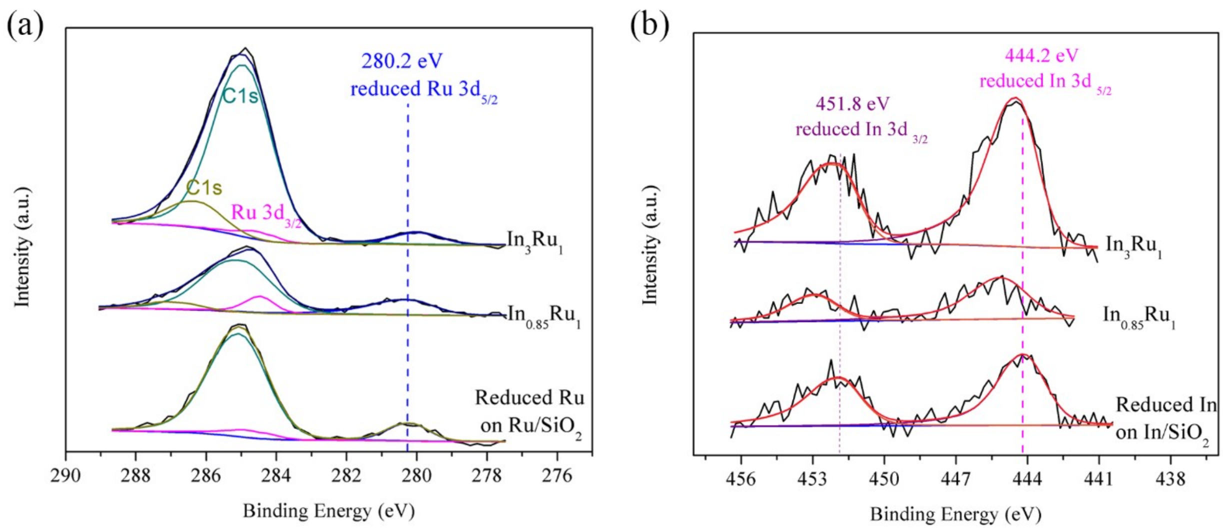

Figure 5. XPS results on (a) Ru3d and C1s region for 800 °C reduced samples (b) In3d region for 800 °C reduced samples The Si $2p_{3/2}$ feature from pure silicon powder at 99.3 eV was used as the reference.

In-situ DRIFTS of Surface Intermediates

In order to provide further insight into the effect of promoters on reaction pathways, adsorption of key reaction intermediates (CO, formate and methoxy) on the catalysts was investigated through in situ DRIFTS experiments. CO adsorption on In-Ru bimetallic catalysts and Ru/SiO_2 was evaluated first at room temperature. As shown in Figure 6 (a), Ru, $In_{0.85}Ru_1$-300, and $In_{0.85}Ru_1$-800 show two CO bands at ~2000 cm^{-1} as CO saturates the sample surface, which is attributed to linearly adsorbed CO.[41] However, bridged CO at ~1800 cm^{-1} was only observed on Ru/SiO_2, and no bridge CO sites were observed on either In-Ru sample.

A DRIFTS study with 1.5 MPa CO_2 on H_2 saturated $In_{0.85}Ru_1$-800 was performed to verify the formation of formate species through CO_2 hydrogenation (Figure 6 (b)). A batch reaction study at similar conditions (CO_2/H_2 = ⅓, 200 ºC and 1 MPa CO_2) was also performed with $In_{0.85}Ru_1$, which resulted in a 91% CH_3OH selectivity with CO and methyl formate as byproducts after a 22h reaction. In the DRIFTS experiment, three bands at 2951, 2868 and 2724 cm^{-1} are visible at 150 ºC. The first band is attributed to the combination of the C-H bending mode and asymmetric stretching of O-C-O of formate while the second and third peaks are attributed to the C-H stretching vibration mode of formate and the combination of C-H bending mode and symmetric stretching of O-C-O of formate, respectively.[42] A broad feature from 1550-1600 cm^{-1} to 1550 cm^{-1} and a band at 1360 cm^{-1} are also observed, which are attributed to asymmetric and symmetric stretching of formate species, respectively.[42, 43] Between the formate region and gas phase CO_2 region (1700-2300 cm^{-1}), features related to high pressure gas phase CO_2 were observed (D, Ea, Ha, Ia, Ja, and Ka bands; Figure S6), which prevented analysis of the adsorbed CO species. [44]

Absorption of formic acid on Ru-800 and In-Ru bimetallic catalysts was performed in the DRIFTS cell to understand the difference between promoters on formate adsorption (Figure. 6 (c)).

The IR result at 200 ^{o}C shows a double peak between 2850 and 2980 cm^{-1}, where the first peak between 2850-2900 cm^{-1} is in the range of a C-H stretching vibration mode of bidentate formate and the peak at higher wavenumber can be attributed to the combination of the C-H bending mode and asymmetric O-C-O stretching mode.[45,46] The C-H stretching vibration mode of formate species over Ru-800 is at 2886 cm^{-1}, while $In_{0.85}Ru_1$-800 and In_3Ru_1-800 exhibit C-H stretching vibration bands at 2867 and 2863 cm^{-1}, respectively which is located ~19 cm^{-1} lower than the Ru-800.

In situ methanol DRIFTS experiments were also performed because methoxy (CH_3O) is suggested as a key reaction intermediate for the methanol synthesis pathway.[47] Methanol adsorption on Ru-800 at 75 ^{o}C results in rapid formation of linearly adsorbed CO (~2000 cm^{-1}) and bridge CO (<1800 cm^{-1}), as shown in Figure 6 (d). The poor stability of methanol on Ru is consistent with our reaction studies in which methanol is not a major product from CO_2 hydrogenation. However, no linear or bridge CO were formed when methanol was adsorbed on the In_3Ru_1-800 catalyst in the temperature range of 75 - 200 ^{o}C (Fig. 6 (e)), showcasing higher methoxy stability due to In incorporation.

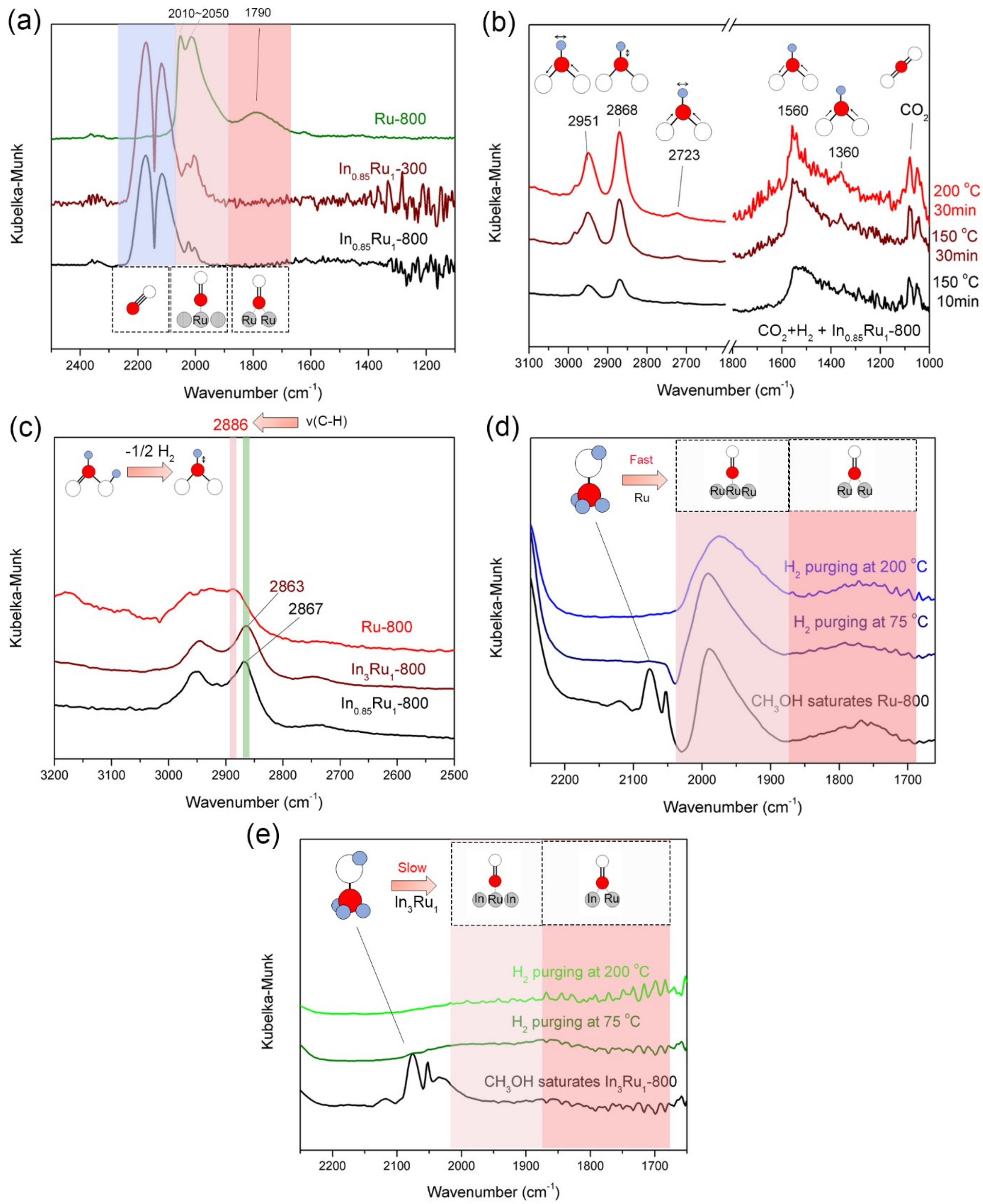

Figure 6. (a) DRIFTS study on CO adsorption over Ru and In-Ru bimetallic catalysts at room temperature (b) CO_2 and H_2 co-adsorption on $In_{0.85}Ru_1$-800 at various temperatures (c) formic acid

adsorption over various catalysts at 200 ºC (d) DRIFTS study on methanol adsorption over Ru-800 at 75 ºC (e) DRIFTS study on methanol adsorption over In_3Ru_1-800 at 75 ºC

DISCUSSION

As depicted in Figures 3 and 4, the addition of the In promoter to Ru significantly alters the methanol selectivity compared to monometallic Ru nanoparticles and results in higher methanol production rates than In_2O_3/SiO_2. Furthermore, In addition prevented methanation of CO_2. To provide more insights to the promotional effects of the In-Ru bimetallic catalysts on the CH_3OH productivities, a clear understanding of the catalyst structure after incorporation of In to Ru was necessary. Thus, the structures of the In_xRu_y-800 bimetallic catalysts were probed by XRD, as shown in Figure 1 (b). After reduction at 800 ºC, the In_3Ru_1 intermetallic phase and residual Ru (101) are both identifiable in the XRD patterns. In_2O_3 was not observed in any of the In_xRu_1 catalysts. The reducibility of In_xRu_1 was then verified by temperature programmed reduction. The primary consumption of H_2 occurred at low temperature (<300 ºC) for Ru and $In_{0.85}Ru_1$. However, materials with higher In/Ru ratios showed multiple H_2 consumption peaks between 400-700 ºC, indicating the reduction of excess In_2O_3 to In at high temperature.[48, 49] These results corroborate the XRD results that show no bulk phase In_2O_3 at reduction temperature of 800 ºC. To further understand the formation process of the In_3Ru_1 intermetallic phase, the final reduction temperature of $In_{0.85}Ru_1$ was varied from 300 ºC to 800 ºC. After reduction at 300 ºC, the XRD pattern shows only one broad diffraction peak located at 42.7º (Figure 2), which is shifted from Ru (101) at 44º. The shift in the diffraction peak towards lower 2θ suggests a larger unit cell size and is rationalized through the dissolution of larger In atoms into the Ru lattice to form an alloy (as depicted in Figure

7). At a reduction temperature of 450 ºC, the In_3Ru_1 intermetallic phase can be identified from XRD, confirming that the solid solution of In and Ru is partially converted into the In_3Ru_1 intermetallic phase. Meanwhile, the previous alloy peak shifts from 42.7º to 43.7º which suggests a smaller unit cell size of In-Ru alloy as In diffuses out of the alloy phase in order to maintain the stoichiometry of the In_3Ru_1 intermetallic compound. With a reduction temperature of 800 ºC, only the In_3Ru_1 phase and Ru (101) facet at 44º can be identified, indicating the conversion of the alloy to the intermetallic phase is completed. The residual Ru phase might be encapsulated in the same way as the core-shell structure of InPd intermetallic and RuFe bimetallic catalyst.[50, 51]

HRTEM and STEM/EDX were then performed on the as-synthesized $In_{0.85}Ru_1$ samples to provide additional structural information. At reduction temperatures of 300 ºC, the nanoparticles were partially crystallized, and the Ru hexagonal close pack (hcp) phase was formed within the particle, as indicated by the HRTEM (Figure S3 and Figure S4 (b)). The EDX results suggest dispersion of In and Ru in the bulk phase with an In content between 27% and 47% on various nanoparticles. At reduction temperatures of 450 ºC, a Janus structure was formed with both the In3Ru1 phase and the Ru phase present within a larger nanoparticle. However, the Ru phase appears to be coated by an amorphous layer (Figure S3 (b)). The EDX mapping on a similar nanoparticle shows the significant In and Ru enrichment on the opposite sides of the particle which was also observed with point scan EDX (Figure S3 (g)). The In content within the small particle was 15% while it was ~70% in the larger particle. This phenomenon was only observed at 450 ºC, and the In content is close to the expected In content in the In_3Ru_1 phase.

A possible formation mechanism is depicted in Figure 7. At 300 ºC, the Ru-enriched region of In-Ru alloy nanoparticles crystallizes as Ru hcp with In present in the entire particle. At a reduction temperature of 450 ºC, the formation of the In_3Ru_1 phase becomes favorable but requires enough In to form In_3Ru_1 phase. Therefore, the In_3Ru_1 phase appears at the relatively In-enriched side of the alloy particle which drives the further accumulation of In. The Ru-enriched region crystallizes in the Ru hcp phase, and the limited solubility of In in Ru phase drives In diffusion out of Ru-enriched portion, especially at higher temperatures. Eventually, these two mechanisms can result in the formation of the Janus structure where the large In_3Ru_1 crystal and small Ru-enriched particles are presented together.

As shown in Figure 3 (a), Ru sites are isolated by In in the In_3Ru_1 intermetallic phase, and the Ru sites are distinct from the Ru hcp phase where Ru atoms form large Ru ensembles. We observe that the near-surface layer of the Ru-enriched alloy nanoparticles in $In_{0.85}Ru_1$-800 have a longer d-spacing compared to the core Ru (Figure S3 (c)), which indicates the presence of In atoms in the lattice. Although EDX cannot resolve the elemental composition on the edge of these particles due to the instability of In-Ru under the electron beam, CO DRIFTS experiments provide additional indirect evidence of Ru isolation. The CO DRIFTS results in Figure 6 (a) show the absence of bridge CO sites for $In_{0.85}Ru_1$ samples which also indicates the In covers the surface and isolates surface Ru. A similar phenomenon has recently been observed with In-Pd alloy nanoparticles. [17]

The performance of these catalysts with different crystal structures is summarized in Figure 4 (a). All three catalysts show CH_3OH selectivity of over 80%, while a significant improvement in the catalytic activity was observed with $In_{0.85}Ru_1$-450. After site normalization of the rates from H_2-O_2 titration experiments, the STY of CH_3OH decreased in the following order: $In_{0.85}Ru_1$-450 > $In_{0.85}Ru_1$-800 > $In_{0.85}Ru_1$-300 (Figure 4 (b)). This indicates the improvement of catalytic activity is not due to the increased amount of accessible Ru, but rather the formation of the In_3Ru_1 intermetallic phase may lead to a higher intrinsic catalytic activity. The In_3Ru_1 phase has a tetragonal crystal structure which is different from the solid solution state of the alloy where In and

Ru are more disordered than the intermetallic phase. Therefore, both geometric and electronic differences of the intermetallic phase may enhance CO_2 reduction. However, the site-normalized CH_3OH production rate of $In_{0.85}Ru_1$-800 is ~2x lower than that of $In_{0.85}Ru_1$-450, and both materials show evidence of the formation of the In_3Ru_1 intermetallic phase. Therefore, the In_3Ru_1 intermetallic phase may not bear sole responsibility for the catalytic improvement. The compositional changes of the surface alloy phase at 450 °C may contribute to the observed promotional effect. Previous work with In-Pd alloys revealed that the near surface layer of In-Pd prepared by deposition of 4 monolayer equivalent (MLE) In on Pd was enriched with a $In_{79}Pd_{21}$ composition. Annealing the sample at 500-600 K resulted in a In/Pd ratio of 1, and the d band of Pd was shifted to resemble a "Cu-like" electronic structure as In/Pd ratio decreases.[52, 53] For the In-Ru alloy, XRD provided indirect evidence that In diffused from the In-Ru alloy as the In_3Ru_1 intermetallic compound was formed at 450 °C. The bulk In/Ru ratio for the remaining part of the alloy compound could be lower than 0.85. Assuming the decline of the In/Ru ratio also occurs on the surface compound of alloy, the electronic structure of the In-Ru alloy can be affected similarly to the transformation from $In_{79}Pd_{21}$ to In_1Pd_1, which may result in an improvement in the catalytic activity. Additional studies on the near surface composition of InRu bimetallic catalyst are in progress to fully understand the promotional effect at 450 °C.

The electronic structure was probed by XPS study on various Ru-800, In-800 and In_xRu_1-800 samples as shown in Figure 5. The In-Ru bimetallic catalysts showed charge transfer with partial reduction of Ru sites and partial oxidation of either Ga or In. The charge transfer was believed to alter adsorption energy of reaction intermediates and decrease the activation barrier for methanol synthesis.[54] However, the binding energy shift is small and may indicate a minor role from electronic effects. Since formate was proposed as a key reaction intermediate for In-based catalysts, the interaction between reaction intermediate and metal sites was further studied through DRIFTS experiments using formic acid on various Ru and In-Ru bimetallic catalysts (Figure 6 (c)). The IR results show the C-H stretching vibration feature of formate was shifted by 19 cm^{-1} from the In-Ru to Ru catalysts. According to Kim et al, the wavenumber shift of the C-H vibration mode of formate is sensitive to the ionicity of formate and can be influenced by the Lewis acidity of the catalyst.[46] The blue shift of the C-H vibration on In-Ru indicates the formate is more stabilized on the surface, as similarly observed on supported Cu catalysts.[46] DFT calculations by Takagiwa et al. predicted that the electronic structure for In_3Ru_1 is tuned by In in terms of band gap and density of states.[21] The resulting stabilization of formate as a surface intermediate from CO_2 hydrogenation may further facilitate CH_3OH synthesis.

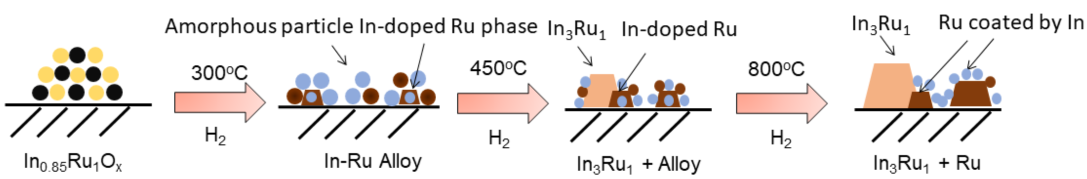

Figure 7. Scheme for structural evolution during reduction at different temperatures

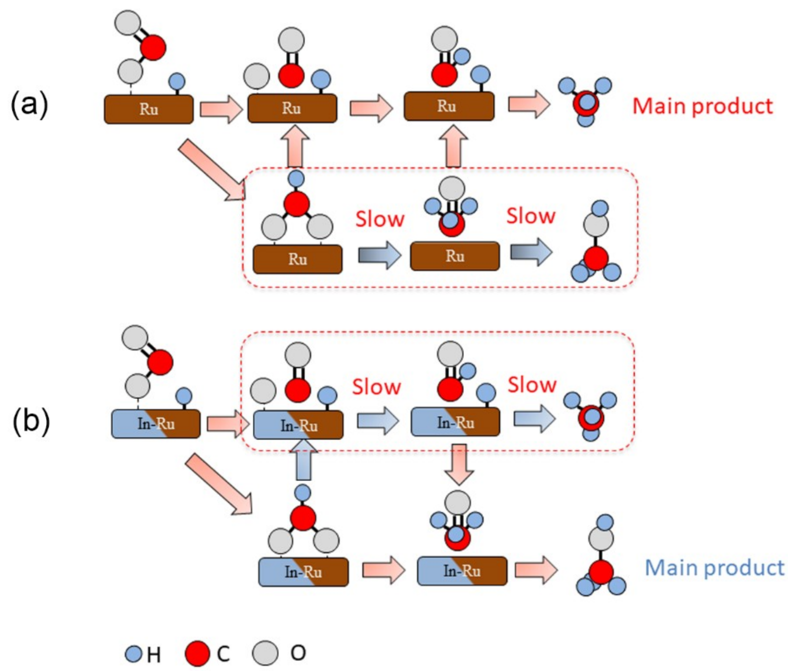

Figure 8. (a) Reaction pathways for CO_2 hydrogenation over Ru nanoparticle and (b) Proposed reaction pathway for CO_2 hydrogenation over In-Ru bimetallic catalysts

The mechanism of CO_2 hydrogenation on supported Ru has been well studied in the literature.[1, 11, 55] In one of the proposed pathways for CO_2 methanation, CO was suggested as a key intermediate.[56, 57] Strong adsorption of CO and the ability to facilitate H_2 dissociation allow Ru to hydrogenate CO into formaldehyde and subsequently convert it to methane (Figure 8 (a)). Formate species, although observed through IR experiments, are not believed to be reaction intermediates for methanation due to slow conversion rates that allow for preferential decomposition into CO rather than proceeding through hydrogenation events to form CH_3OH. [11, 58]

As shown in the CO DRIFTS experiments (Figure 6 (a)), the CO adsorbed on $In_{0.85}Ru_1$ is in the form of linear CO, which indicates the lack of bridge Ru sites. Similar observations on In-Pd alloy have been reported, and DFT calculations revealed that CO dissociation on isolated Pd sites has a higher energy barrier than pure Pd.[17] Similarly, CO adsorption and dissociation on isolated Ru sites can be more difficult as a result of In incorporation. Secondly, H_2-D_2 exchange experiments were performed (see Figure S4 (a) and (b)) and show that H_2 activation can be observed at sub-ambient temperature over Ru-800 while no exchange can be observed on In_3Ru_1-800. The observation is in agreement with the DFT calculations on In-Pd alloys in which In incorporation increases the energy barrier for H_2 dissociation.[17] In addition, a CO-TPRx experiment was also performed on the In_3Ru_1-800 and Ru-800 catalysts. Significant methane was detected with Ru-800 starting from 75 ^oC, while no methane was formed with In_3Ru_1-800 (Figure S5). Thus, the current evidence showcases that the addition of In can influence multiple steps in the methanation pathway whereby inhibiting methanation from occurring.

For the CH_3OH synthesis pathway, it has been proposed to proceed through either a CO or formate intermediate.[59] Through the DRIFTS CO_2/H_2 co-adsorption experiment, the results indicate formate is produced with $In_{0.85}Ru_1$-800 at temperatures as low as 150 ^oC (Figure 6 (b)). The stability of methoxy on Ru and In-Ru bimetallic catalyst was also investigated through methanol adsorption experiments (Figure 6 (d) and (e)), which showed strong evidence of CO formation on Ru/SiO_2, while no CO was not observed on In_3Ru_1. Goodman and coworkers previously reported the decomposition of formaldehyde to H_2, CO and even CH_4 on Ru.[60] The observed linear and bridge CO on Ru may result from CH_3OH dehydrogenation and subsequent decomposition of formaldehyde. Thus, the stability of methanol is low on Ru/SiO_2 and can be converted into CH_4 through CO hydrogenation. However, our findings reveal the distinct nature of the Ru sites in the In-Ru catalysts that stabilize methoxy species. The solvent environment may also help prevent the decomposition of methanol. [61] Considering the solvent-solute interactions and the high solubility of methanol in 1,4-dioxane to facilitate the desorption of methanol from the catalyst surface, the reactivity of methanol may decrease in 1,4-dioxane compared to the gas phase. Therefore, it is speculated that hydrogenation of CO_2 to formate and subsequent hydrogenation steps to methoxy species (Figure 8 (b)) is more favorable on In-Ru than Ru, resulting in higher CH_3OH selectivity.

Conclusion

Monometallic Ru catalysts are well known catalysts used to form methane from H_2/CO_2. Here, we found that In is effective promoters to prevent methanation, with observed CH_3OH selectivity >85 % with In incorporation. Addition of In strengthens the charge transfer from the surface to formate species to increase its stability. Further, In modulates Ru and hinders the activation of H_2 and the adsorption/hydrogenation of CO to CH_4. Lastly, In addition prevents the aggressive decomposition of CH_3OH to CO, which occurs on monometallic Ru nanoparticles. Theoretical calculations are needed to fully understand the influence of In on the various reaction pathways for these interesting and remarkably selective CH_3OH synthesis catalysts. Overall, these results showcase inhibition of reaction pathways through promoter incorporation and provide another subclass of Ru-based materials to interrogate for selective CO_2 reduction processes, which could open up new opportunities for the rational design of catalysts for methanol synthesis.

ASSOCIATED CONTENT

Supporting Information.

The Supporting Information is available free of charge at DOI XXX

Synthesis procedure for In_2O_3 and $In_1Ni_{0.9}$, ICP-OES results, representative carbon balance, HRTEM and EDX results for $In_{0.85}Ru_1$ bimetallic catalysts, DRIFTS result in CO_2 hydrogenation, isotherm curves for H_2-O_2 titration on $In_{0.85}Ru_1$, H_2-D_2 exchange experiment and CO-TPRx results.

AUTHOR INFORMATION

Corresponding Author

*Email: Jhicks3@nd.edu

ORCID

Jason C. Hicks: 0000-0002-5054-2874

ACKNOWLEDGMENT

This work was supported in part by the NSF CAREER Award CBET-1351609, Defense University Research Instrumentation Program under AFOSR Award No. FA9550-17-1-0376 and the Center for Environmental Science and Technology at Notre Dame (CEST). The authors also thank the Material Characterization Facility at Notre Dame (MCF) for the use of XRD and XPS and CEST for the use of the ICP-OES.

REFERENCES

1. Guo, Y.; Mei, S.; Yuan, K.; Wang, D.-J.; Liu, H.-C.; Yan, C.-H.; Zhang, Y.-W., Low-Temperature CO_2 Methanation over CeO_2-Supported Ru Single Atoms, Nanoclusters, and Nanoparticles Competitively Tuned by Strong Metal–Support Interactions and H-Spillover Effect. *ACS Catalysis* **2018,** *8* (7), 6203-6215. doi:10.1021/acscatal.7b04469

2. Jiang, X.; Nie, X.; Guo, X.; Song, C.; Chen, J. G., Recent Advances in Carbon Dioxide Hydrogenation to Methanol via Heterogeneous Catalysis. *Chemical Reviews* **2020,** *120* (15), 7984-8034. doi:10.1021/acs.chemrev.9b00723

3. Nie, X.; Jiang, X.; Wang, H.; Luo, W.; Janik, M. J.; Chen, Y.; Guo, X.; Song, C., Mechanistic Understanding of Alloy Effect and Water Promotion for Pd-Cu Bimetallic Catalysts in CO_2 Hydrogenation to Methanol. *ACS Catalysis* **2018,** *8* (6), 4873-4892. doi:10.1021/acscatal.7b04150

4. Lin, F.; Jiang, X.; Boreriboon, N.; Wang, Z.; Song, C.; Cen, K., Effects of supports on bimetallic Pd-Cu catalysts for CO_2 hydrogenation to methanol. *Applied Catalysis A: General* **2019,** *585*, 117210. doi:10.1016/j.apcata.2019.117210

5. Liu, R.; Leshchev, D.; Stavitski, E.; Juneau, M.; Agwara, J. N.; Porosoff, M. D., Selective hydrogenation of CO_2 and CO over potassium promoted Co/ZSM-5. *Applied Catalysis B: Environmental* **2021,** *284*, 119787. doi:10.1016/j.apcatb.2020.119787

6. Ahmad, K.; Upadhyayula, S., Greenhouse gas CO_2 hydrogenation to fuels: A thermodynamic analysis. *Environmental Progress & Sustainable Energy* **2019,** *38* (1), 98-111. doi:10.1002/ep.13028

7. Alvarez, A.; Bansode, A.; Urakawa, A.; Bavykina, A. V.; Wezendonk, T. A.; Makkee, M.; Gascon, J.; Kapteijn, F., Challenges in the Greener Production of Formates/Formic Acid, Methanol, and DME by Heterogeneously Catalyzed CO_2 Hydrogenation Processes. *Chem Rev* **2017,** *117* (14), 9804-9838. doi:10.1021/acs.chemrev.6b00816

8. Porosoff, M. D.; Yan, B.; Chen, J. G., Catalytic reduction of CO_2 by H_2 for synthesis of CO, methanol and hydrocarbons: challenges and opportunities. *Energy & Environmental Science* **2016,** *9* (1), 62-73. doi:10.1039/c5ee02657a

9. Li, M. M.; Zou, H.; Zheng, J.; Wu, T. S.; Chan, T. S.; Soo, Y. L.; Wu, X. P.; Gong, X. Q.; Chen, T.; Roy, K.; Held, G.; Tsang, S. C. E., Methanol Synthesis at a Wide Range of H_2 /CO_2 Ratios over a Rh-In Bimetallic Catalyst. *Angew Chem Int Ed Engl* **2020,** *59* (37), 16039-16046. doi:10.1002/anie.202000841

10. Kelley, R. D.; Goodman, D. W., Catalytic methanation over single crystal nickel and ruthenium: Reaction kinetics on different crystal planes and the correlation of surface carbide concentration with reaction rate. *Surface Science* **1982,** *123* (2), L743-L749. doi:10.1016/0039-6028(82)90319-3

11. Miao, B.; Ma, S. S. K.; Wang, X.; Su, H.; Chan, S. H., Catalysis mechanisms of CO_2 and CO methanation. *Catalysis Science & Technology* **2016,** *6* (12), 4048-4058. doi:10.1039/c6cy00478d

12. Abe, T.; Tanizawa, M.; Watanabe, K.; Taguchi, A., CO_2 methanation property of Ru nanoparticle-loaded TiO_2 prepared by a polygonal barrel-sputtering method. *Energy & Environmental Science* **2009,** *2* (3), 315-321. doi:10.1039/b817740f

13. Sharma, S.; Hu, Z.; Zhang, P.; McFarland, E. W.; Metiu, H., CO_2 methanation on Ru-doped ceria. *Journal of Catalysis* **2011,** *278* (2), 297-309. doi:10.1016/j.jcat.2010.12.015

14. Wesselbaum, S.; Moha, V.; Meuresch, M.; Brosinski, S.; Thenert, K. M.; Kothe, J.; vom Stein, T.; Englert, U.; Hölscher, M.; Klankermayer, J., Hydrogenation of carbon dioxide to

methanol using a homogeneous ruthenium–Triphos catalyst: from mechanistic investigations to multiphase catalysis. *Chemical science* **2015,** *6* (1), 693-704. doi:10.1039/C4SC02087A

15. Xu, Z.; McNamara, N. D.; Neumann, G. T.; Schneider, W. F.; Hicks, J. C., Catalytic Hydrogenation of CO_2 to Formic Acid with Silica-Tethered Iridium Catalysts. *ChemCatChem* **2013,** *5* (7), 1769-1771. doi:10.1002/cctc.201200839

16. McNamara, N. D.; Hicks, J. C., CO_2 Capture and Conversion with a Multifunctional Polyethyleneimine-Tethered Iminophosphine Iridium Catalyst/Adsorbent. *ChemSusChem* **2014,** *7* (4), 1114-1124. doi:10.1002/cssc.201301231

17. Ye, J.; Ge, Q.; Liu, C.-j., Effect of PdIn bimetallic particle formation on CO_2 reduction over the Pd–In/SiO_2 catalyst. *Chemical Engineering Science* **2015,** *135*, 193-201. doi:10.1016/j.ces.2015.04.034

18. Snider, J. L.; Streibel, V.; Hubert, M. A.; Choksi, T. S.; Valle, E.; Upham, D. C.; Schumann, J.; Duyar, M. S.; Gallo, A.; Abild-Pedersen, F.; Jaramillo, T. F., Revealing the Synergy between Oxide and Alloy Phases on the Performance of Bimetallic In–Pd Catalysts for CO_2 Hydrogenation to Methanol. *ACS Catalysis* **2019,** *9* (4), 3399-3412. doi:10.1021/acscatal.8b04848

19. Holleck, H.; Nowotny, H.; Benesovsky, F., Die Kristallstruktur von $ThGa_2$ und $RuIn_3$. *Monatshefte für Chemie und verwandte Teile anderer Wissenschaften* **1964,** *95* (4), 1386-1390. doi:10.1007/BF00904736

20. Okamoto, H.; Massalski, T., *Binary alloy phase diagrams*. ASM International: Materials Park, OH, USA, 1990; Vol. 9, p 6.

21. Takagiwa, Y.; Kitahara, K.; Matsubayashi, Y.; Kimura, K., Thermoelectric properties of FeGa3-type narrow-bandgap intermetallic compounds Ru(Ga,In)3: Experimental and calculational studies. *Journal of Applied Physics* **2012,** *111* (12), 123707. doi:10.1063/1.4729772

22. Pöttgen, R., Preparation, crystal structure and properties of $RuIn_3$. *Journal of Alloys and Compounds* **1995,** *226* (1), 59-64. doi:10.1016/0925-8388(95)01575-2

23. Kubicka, H., Hydrogen adsorption and hydrogen-oxygen titration on ruthenium powder. *Reaction Kinetics and Catalysis Letters* **1976,** *5* (2), 223-228. doi:10.1007/BF02279794

24. Muhler, M.; Nielsen, L. P.; Törnqvist, E.; Clausen, B. S.; Topsøe, H., Temperature-programmed desorption of H_2 as a tool to determine metal surface areas of Cu catalysts. *Catalysis Letters* **1992,** *14* (3), 241-249. doi:10.1007/BF00769661

25. Chen, Y.; Choi, S.; Thompson, L. T., Low-Temperature CO_2 Hydrogenation to Liquid Products via a Heterogeneous Cascade Catalytic System. *ACS Catal.* **2015,** *5* (3), 1717-1725. doi:10.1021/cs501656x

26. Chen, Y.; Choi, S.; Thompson, L. T., Low temperature CO_2 hydrogenation to alcohols and hydrocarbons over Mo_2C supported metal catalysts. *J. Catal.* **2016,** *343,* 147-156. doi:10.1016/j.jcat.2016.01.016

27. Wiedner, E. S.; Chambers, M. B.; Pitman, C. L.; Bullock, R. M.; Miller, A. J.; Appel, A. M., Thermodynamic Hydricity of Transition Metal Hydrides. *Chem Rev* **2016,** *116* (15), 8655-92. doi:10.1021/acs.chemrev.6b00168

28. Wiedner, E. S.; Linehan, J. C., Making a Splash in Homogeneous CO_2 Hydrogenation: Elucidating the Impact of Solvent on Catalytic Mechanisms. *Chemistry* **2018,** *24* (64), 16964-16971. doi:10.1002/chem.201801759

29. Joó, F.; Joó, F.; Nádasdi, L.; Elek, J.; Laurenczy, G.; Nádasdi, L., Homogeneous hydrogenation of aqueous hydrogen carbonate to formate under exceedingly mild conditions—a novel possibility of carbon dioxide activation†. *Chemical Communications* **1999,** (11), 971-972. doi:10.1039/A902368B

30. Geldbach, T. J.; Laurenczy, G.; Scopelliti, R.; Dyson, P. J., Synthesis of Imidazolium-Tethered Ruthenium(II)-Arene Complexes and Their Application in Biphasic Catalysis. *Organometallics* **2006,** *25* (3), 733-742. doi:10.1021/om050849u

31. Hara, T.; Nguyen, H. T.; Komiyama, M., Facile and Green Decomposition of Dioxane with Catalytic Supercritical Water Gasification. *Chemistry Letters* **2014,** *43* (10), 1628-1630. doi:10.1246/cl.140611

32. Jain, A.; Ong, S. P.; Hautier, G.; Chen, W.; Richards, W. D.; Dacek, S.; Cholia, S.; Gunter, D.; Skinner, D.; Ceder, G.; Persson, K. A., Commentary: The Materials Project: A materials genome approach to accelerating materials innovation. *APL Materials* **2013,** *1* (1), 011002. doi:10.1063/1.4812323

33. García-Trenco, A.; Regoutz, A.; White, E. R.; Payne, D. J.; Shaffer, M. S. P.; Williams, C. K., PdIn intermetallic nanoparticles for the Hydrogenation of CO_2 to Methanol. *Applied Catalysis B: Environmental* **2018,** *220*, 9-18. doi:10.1016/j.apcatb.2017.07.069

34. Martin, O.; Martin, A. J.; Mondelli, C.; Mitchell, S.; Segawa, T. F.; Hauert, R.; Drouilly, C.; Curulla-Ferre, D.; Perez-Ramirez, J., Indium Oxide as a Superior Catalyst for Methanol Synthesis by CO_2 Hydrogenation. *Angew Chem Int Ed Engl* **2016,** *55* (21), 6261-5. doi:10.1002/anie.201600943

35. Duyar, M. S.; Tsai, C.; Snider, J. L.; Singh, J. A.; Gallo, A.; Yoo, J. S.; Medford, A. J.; Abild-Pedersen, F.; Studt, F.; Kibsgaard, J.; Bent, S. F.; Nørskov, J. K.; Jaramillo, T. F., A Highly Active Molybdenum Phosphide Catalyst for Methanol Synthesis from CO and CO_2. *Angew. Chem. Int. Ed Engl.* **2018,** *130* (46), 15265-15270. doi:10.1002/ange.201806583

36. Chang, K.; Wang, T.; Chen, J. G., Hydrogenation of CO_2 to methanol over $CuCeTiO_x$ catalysts. *Applied Catalysis B: Environmental* **2017,** *206*, 704-711. doi:10.1016/j.apcatb.2017.01.076

37. Chen, M.; Xu, J.; Cao, Y.; He, H.-Y.; Fan, K.-N.; Zhuang, J.-H., Dehydrogenation of propane over In2O3–Al2O3 mixed oxide in the presence of carbon dioxide. *Journal of Catalysis* **2010,** *272* (1), 101-108. doi:10.1016/j.jcat.2010.03.007

38. Alexander V, N.; Anna, K.-V.; Stephen W, G.; Cedric J, P. NIST X-ray Photoelectron Spectroscopy Database. https://srdata.nist.gov/xps/.(accessed 03/2021).

39. Guo, S.; Heck, K.; Kasiraju, S.; Qian, H.; Zhao, Z.; Grabow, L. C.; Miller, J. T.; Wong, M. S., Insights into Nitrate Reduction over Indium-Decorated Palladium Nanoparticle Catalysts. *ACS Catalysis* **2018,** *8* (1), 503-515. doi:10.1021/acscatal.7b01371

40. Ogawa, T.; Kobayashi, Y.; Mizoguchi, H.; Kitano, M.; Abe, H.; Tada, T.; Toda, Y.; Niwa, Y.; Hosono, H., High Electron Density on Ru in Intermetallic YRu_2: The Application to

Catalyst for Ammonia Synthesis. *The Journal of Physical Chemistry C* **2018,** *122* (19), 10468-10475. doi:10.1021/acs.jpcc.8b02128

41. Chin, S. Y.; Williams, C. T.; Amiridis, M. D., FTIR Studies of CO Adsorption on Al2O3- and SiO2-Supported Ru Catalysts. *The Journal of Physical Chemistry B* **2006,** *110* (2), 871-882. doi:10.1021/jp053908q

42. Wang, J.; Li, G.; Li, Z.; Tang, C.; Feng, Z.; An, H.; Liu, H.; Liu, T.; Li, C., A highly selective and stable ZnO-ZrO_2 solid solution catalyst for CO_2 hydrogenation to methanol. *Science Advances* **2017,** *3* (10), e1701290. doi:10.1126/sciadv.1701290

43. Weigel, J.; Koeppel, R. A.; Baiker, A.; Wokaun, A., Surface Species in CO and CO_2 Hydrogenation over Copper/Zirconia: On the Methanol Synthesis Mechanism. *Langmuir* **1996,** *12* (22), 5319-5329. doi:10.1021/la9506990

44. Fehr, S. M.; Krossing, I., Spectroscopic Signatures of Pressurized Carbon Dioxide in Diffuse Reflectance Infrared Spectroscopy of Heterogeneous Catalysts. *ChemCatChem* **2020,** *12* (9), 2622-2629. doi:10.1002/cctc.201902038

45. Nanayakkara, C. E.; Dillon, J. K.; Grassian, V. H., Surface Adsorption and Photochemistry of Gas-Phase Formic Acid on TiO_2 Nanoparticles: The Role of Adsorbed Water in Surface Coordination, Adsorption Kinetics, and Rate of Photoproduct Formation. *The Journal of Physical Chemistry C* **2014,** *118* (44), 25487-25495. doi:10.1021/jp507551y

46. Kim, J.; Sarma, B. B.; Andrés, E.; Pfänder, N.; Concepción, P.; Prieto, G., Surface Lewis Acidity of Periphery Oxide Species as a General Kinetic Descriptor for CO2 Hydrogenation

to Methanol on Supported Copper Nanoparticles. *ACS Catalysis* **2019,** *9* (11), 10409-10417. doi:10.1021/acscatal.9b02412

47. Solis-Garcia, A.; Louvier-Hernandez, J. F.; Almendarez-Camarillo, A.; Fierro-Gonzalez, J. C., Participation of surface bicarbonate, formate and methoxy species in the carbon dioxide methanation catalyzed by ZrO_2-supported Ni. *Applied Catalysis B: Environmental* **2017,** *218*, 611-620. doi:10.1016/j.apcatb.2017.06.063

48. Onyestyák, G., Ni/silica-based bimetallic catalysts by solid-state co-reduction of admixed metal oxides for acetic acid hydroconversion to ethanol. *Research on Chemical Intermediates* **2015,** *41* (12), 9207-9215. doi:10.1007/s11164-015-1957-x

49. Chen, M.; Wu, J.-L.; Liu, Y.-M.; Cao, Y.; Guo, L.; He, H.-Y.; Fan, K.-N., Study in support effect of In_2O_3/MO_x (M= Al, Si, Zr) catalysts for dehydrogenation of propane in the presence of CO_2. *Applied Catalysis A: General* **2011,** *407* (1-2), 20-28. doi:10.1016/j.apcata.2011.08.018

50. Wu, Z.; Wegener, E. C.; Tseng, H.-T.; Gallagher, J. R.; Harris, J. W.; Diaz, R. E.; Ren, Y.; Ribeiro, F. H.; Miller, J. T., Pd–In intermetallic alloy nanoparticles: highly selective ethane dehydrogenation catalysts. *Catalysis Science & Technology* **2016,** *6* (18), 6965-6976. doi:10.1039/c6cy00491a

51. Aitbekova, A.; Goodman, E. D.; Wu, L.; Boubnov, A.; Hoffman, A. S.; Genc, A.; Cheng, H.; Casalena, L.; Bare, S. R.; Cargnello, M., Engineering of Ruthenium–Iron Oxide Colloidal Heterostructures: Improved Yields in CO_2 Hydrogenation to Hydrocarbons. *Angewandte Chemie International Edition* **2019,** *58* (48), 17451-17457. doi:10.1002/anie.201910579

52. McGuirk, G. M.; Ledieu, J.; Gaudry, É.; de Weerd, M. C.; Fournée, V., Surface structures of In-Pd intermetallic compounds. I. Experimental study of In thin films on Pd(111) and alloy formation. *The Journal of Chemical Physics* **2014,** *141* (8), 084702. doi:10.1063/1.4892408

53. Rameshan, C.; Lorenz, H.; Mayr, L.; Penner, S.; Zemlyanov, D.; Arrigo, R.; Haevecker, M.; Blume, R.; Knop-Gericke, A.; Schlögl, R., CO_2-selective methanol steam reforming on In-doped Pd studied by in situ X-ray photoelectron spectroscopy. *Journal of catalysis* **2012,** *295*, 186-194. doi:10.1016/j.jcat.2012.08.008

54. Vidal, A. B.; Feria, L.; Evans, J.; Takahashi, Y.; Liu, P.; Nakamura, K.; Illas, F.; Rodriguez, J. A., CO_2 Activation and Methanol Synthesis on Novel Au/TiC and Cu/TiC Catalysts. *The Journal of Physical Chemistry Letters* **2012,** *3* (16), 2275-2280. doi:10.1021/jz300989e

55. Kwak, J. H.; Kovarik, L.; Szanyi, J., CO_2 Reduction on Supported Ru/Al_2O_3 Catalysts: Cluster Size Dependence of Product Selectivity. *ACS Catalysis* **2013,** *3* (11), 2449-2455. doi:10.1021/cs400381f

56. Janke, C.; Duyar, M. S.; Hoskins, M.; Farrauto, R., Catalytic and adsorption studies for the hydrogenation of CO_2 to methane. *Applied Catalysis B: Environmental* **2014,** *152-153*, 184-191. doi:10.1016/j.apcatb.2014.01.016

57. Ren, J.; Guo, H.; Yang, J.; Qin, Z.; Lin, J.; Li, Z., Insights into the mechanisms of CO_2 methanation on Ni(111) surfaces by density functional theory. *Applied Surface Science* **2015,** *351*, 504-516. doi:10.1016/j.apsusc.2015.05.173

58. Solymosi, F.; Erdöhelyi, A.; Kocsis, M., Methanation of CO_2 on supported Ru catalysts. *Journal of the Chemical Society, Faraday Transactions 1: Physical Chemistry in Condensed Phases* **1981,** *77* (5), 1003-1012. doi:10.1039/F19817701003

59. Grabow, L. C.; Mavrikakis, M., Mechanism of Methanol Synthesis on Cu through CO_2 and CO Hydrogenation. *ACS Catal.* **2011,** *1* (4), 365-384. doi:10.1021/cs200055d

60. Goodman, D. W.; Madey, T. E.; Ono, M.; Yates, J. T., Interaction of hydrogen, carbon monoxide, and formaldehyde with ruthenium. *Journal of Catalysis* **1977,** *50* (2), 279-290. doi:10.1016/0021-9517(77)90037-9

61. Dyson, P. J.; Jessop, P. G., Solvent effects in catalysis: rational improvements of catalysts via manipulation of solvent interactions. *Catalysis Science & Technology* **2016,** *6* (10), 3302-3316. doi:10.1039/c5cy02197a

TOC FIGURE:

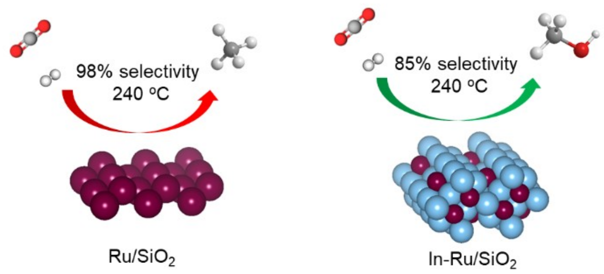

Synopsis: Promotion of Ru with In inhibits methane formation during CO_2 reduction and shifts selectivity to methanol .